Available online at www.sciencedirect.com

ScienceDirect

Acta Materialia 59 (2011) 658–670

Acta MATERIALIA

www.elsevier.com/locate/actamat

Deformation and fracture mechanisms in fine- and ultrafine-grained ferrite/martensite dual-phase steels and the effect of aging

Marion Calcagnotto [a], Yoshitaka Adachi [b], Dirk Ponge [a], Dierk Raabe [a,*]

[a] *Max-Planck-Institut für Eisenforschung GmbH, Max-Planck-Straße 1, 40237 Düsseldorf, Germany*
[b] *National Institute for Materials Science, 1-2-1 Sengen, Tsukuba, Ibaraki 305-0047, Japan*

Received 23 August 2010; received in revised form 29 September 2010; accepted 1 October 2010

Abstract

Three ferrite/martensite dual-phase steels varying in the ferrite grain size (12.4, 2.4 and 1.2 μm) but with the same martensite content (~30 vol.%) were produced by large-strain warm deformation at different deformation temperatures, followed by intercritical annealing. Their mechanical properties were compared, and the response of the ultrafine-grained steel (1.2 μm) to aging at 170 °C was investigated. The deformation and fracture mechanisms were studied based on microstructure observations using scanning electron microscopy and electron backscatter diffraction. Grain refinement leads to an increase in both yield strength and tensile strength, whereas uniform elongation and total elongation are less affected. This can be partly explained by the increase in the initial strain-hardening rate. Moreover, the stress/strain partitioning characteristics between ferrite and martensite change due to grain refinement, leading to enhanced martensite plasticity and better interface cohesion. Grain refinement further promotes ductile fracture mechanisms, which is a result of the improved fracture toughness of martensite. The aging treatment leads to a strong increase in yield strength and improves the uniform and total elongation. These effects are attributed to dislocation locking due to the formation of Cottrell atmospheres and relaxation of internal stresses, as well as to the reduction in the interstitial carbon content in ferrite and tempering effects in martensite.

Keywords: Ultrafine grains; Dual-phase steel; Aging; Deformation mechanisms; Fracture mechanisms

1. Introduction

Grain refinement of metals is essential as it is the only strengthening mechanism that simultaneously enhances the toughness of a material. In recent years, a variety of methods have been developed to produce ultrafine-grained (UFG) materials with a ferrite grain size of around 1 μm [1,2]. These methods can be divided into advanced thermomechanical processing (ATMP) routes, which aim at improving conventional processing routes in commercial large-scale rolling mills, and severe plastic deformation (SPD) techniques, which are essentially confined to laboratory-scale sample dimensions. The ATMP methods cover deformation-induced ferrite transformation (DIFT) [3], large-strain warm deformation [4], intercritical hot rolling [5], multi-directional rolling [6] and cold-rolling plus annealing of martensitic steel [7]. The most important SPD techniques are equal-channel angular pressing (ECAP) [8], accumulative roll bonding [9] and high-pressure torsion [10].

It was consistently found that yield strength and tensile strength are drastically increased due to grain refinement, whereas uniform and total elongation are decreased. Also, Lüders straining becomes more pronounced. Furthermore, UFG steels exhibit a very low strain-hardening rate [11], which marks the main limitation with respect to commercial applications. In terms of toughness, a significant reduction in the ductile-to-brittle transition temperature

---

* Corresponding author. Tel.: +49 211 6792 340; fax: +49 211 6792 333.
E-mail address: d.raabe@mpie.de (D. Raabe).

1359-6454/$36.00 © 2010 Acta Materialia Inc. Published by Elsevier Ltd. All rights reserved.
doi:10.1016/j.actamat.2010.10.002

has been repeatedly reported [12,13]. For these reasons, it is of ongoing interest to overcome the restricted ductility of UFG materials without sacrificing strength and toughness. Among the possible ways to restore the strain hardenability of UFG materials are the fabrication of a bimodal grain size distribution [14] and the introduction of nanosized cementite particles into the microstructure [6]. Another aspect that might improve the applicability of UFG materials is their ability to show superplasticity [15]. Shin and Park [16] showed that replacing cementite as a second phase by martensite through an intercritical annealing treatment leads to a substantial increase in strain-hardening rate, causing a higher ultimate tensile strength with only slightly reduced uniform and total elongation. In this way, a UFG ferrite/martensite dual-phase (DP) steel was designed which shows superior mechanical properties compared to coarser grained conventional DP steels. The term “dual-phase steel” refers to a group of steels consisting of a soft ferrite matrix and 3–30 vol.% of hard martensite islands. These steels are widely used for automotive applications. DP steels have a number of unique properties, which include a low elastic limit, high initial strain-hardening rate, continuous yielding, high tensile strength and high uniform and total elongation. Moreover, DP steels exhibit a bake-hardening (BH) effect, i.e. the yield strength increases upon aging at paint-baking temperatures (~170 °C) after forming, giving rise to improved dent and crush resistance. The austenite-to-martensite phase transformation bears the main influence on the mechanical properties of dual-phase steels [17,18]. This phase transformation involves a volume expansion of 2–4% [19], causing an elastically and plastically deformed zone in the ferrite adjacent to martensite [20]. The deformed zone contains a high number of unpinned dislocations [21], giving rise to dislocation heterogeneities in the ferrite. The low elastic limit is thus suggested to be generated by the combined effects of the present elastic stresses that facilitate plastic flow and the additional dislocation, which is assumed to be partly mobile during early stages of yielding [22]. Dislocation–dislocation interactions, dislocation pile-ups at ferrite/martensite interfaces and the corresponding long-range elastic back stresses contribute to rapid strain hardening.

Previous studies on grain refinement in DP steels consistently revealed that, unlike in other metallic materials, the increases in yield strength and tensile strength are not counteracted by a significant reduction in the uniform and total elongation [23–28]. This can partly be explained by the enhanced strain-hardening rate due to grain refinement as a result of the higher number of geometrically necessary dislocations (GNDs) along the ferrite–martensite boundaries [25]. Ultrafine-grained DP steels have been produced by applying a two-step processing route consisting of (1) a deformation treatment to produce UFG ferrite and finely dispersed cementite or pearlite and (2) a short intercritical annealing in the ferrite/austenite two-phase field followed by quenching to transform all austenite to martensite. Grain refinement in step (1) was achieved by ECAP [27], cold rolling [28], cold swaging [24] and large-strain warm deformation [29]. A single-pass processing route based on DIFT was proposed by Mukherjee et al. [26,30].

As the number of investigations on this topic is very limited, more research is required to understand the mechanical response of DP steels to ferrite grain sizes close to or below 1 μm. Furthermore, as the microstructures described in the previous studies often differ in the martensite volume fraction, it has not been possible to interpret the grain size effect on the mechanical properties independently so far. Therefore, in this study we compare the deformation and fracture mechanisms of a coarse-grained (CG), a fine-grained (FG) and a UFG-DP steel, having about the same martensite volume fractions. In addition, the aging (BH) response of the UFG-DP steel is investigated, which has not been addressed so far. In conjunction with the mechanical data, the microstructure evolution during tensile straining and the fracture mechanisms are studied by using scanning electron microscopy (SEM) and high-resolution electron backscatter diffraction (EBSD). Furthermore, slip-band evolution during deformation was investigated by performing tensile tests which were interrupted at strain levels between 1% and 4%.

2. Experimental procedures

2.1. Materials processing

A plain carbon manganese steel of composition (in wt.%) 0.17 C, 1.49 Mn, 0.22 Si, 0.033 Al, 0.0033 N, 0.0017 P and 0.0031 S was produced by vacuum induction melting. A lean composition was selected in order to show that a stable ferrite grain size of around 1 μm can be achieved via thermomechanical processing without microalloying. Carbon enhances both grain refinement and grain size stability [31]. At the same time, the carbon content has to be low enough to ensure good weldability, which is fulfilled for carbon contents below 0.2%. Mn was also shown to be highly beneficial for the grain refinement process [32]. Furthermore, it increases the hardenability and lowers the Ar_3 temperature [29]. However, too high a Mn content will promote segregation and undesired banded microstructures. Samples ($50 \times 40 \times 60\ mm^3$) for thermomechanical processing were machined directly from the cast ingot. The thermomechanical processing was realized by use of a large-scale 2.5 MN hot deformation simulator [4,33,34]. This computer-controlled servohydraulic press allows the simulation of industrial hot-rolling processing routes by performing multi-step flat compression tests. The processing schedules to obtain three different grain sizes are outlined in Fig. 1.

The first step is identical for all processing schedules. It consists of 3 min of reaustenitization at 912 °C and a single-pass deformation at 860 °C applying a logarithmic strain of $\varepsilon = 0.3$ at a strain rate of $10\ s^{-1}$ above the recrystallization temperature. In the CG route (Fig. 1a),

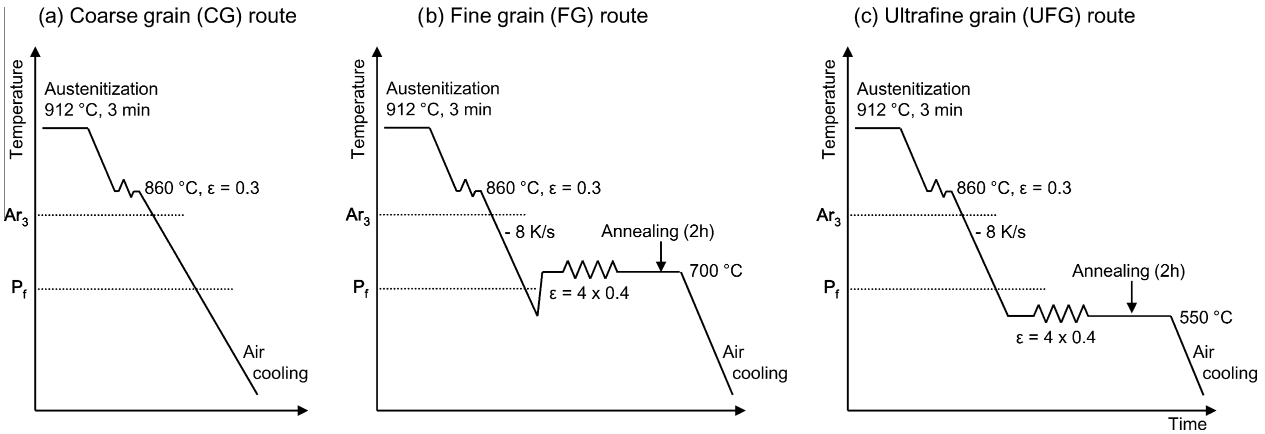

Fig. 1. Thermomechanical processing routes to produce different grain sizes in a hot deformation simulator. All treatments are followed by an intercritical annealing at 730 °C for 3 min and subsequent quenching to obtain the final ferrite/martensite dual-phase microstructure. Ar_3: non-equilibrium transformation start temperature; P_f: pearlite transformation finish temperature; ε: logarithmic strain.

the sample is then air cooled to room temperature to obtain a conventional ferrite–pearlite starting microstructure. Grain refinement is achieved by subsequent large-strain warm deformation at 700 °C (the FG route, Fig. 1b) and at 550 °C (the UFG route, Fig. 1c), respectively. A total strain of 1.6 is realized by a four-step flat compression series, each step exerting a strain of 0.4 at a strain rate of 10 s^{-1}. The deformation temperature controls the degree of grain refinement. At 700 °C, a fine polygonal ferrite matrix with globular cementite and fine pearlite colonies is formed. At 550 °C, continuous grain subdivision and pronounced recovery lead to slightly elongated ferrite grains with a grain size of around 1 μm [4]. The cementite lamellae of the pearlite colonies undergo continuous fragmentation and spheroidization. This results in a fine distribution of spheroidized cementite particles which mainly cover the ferrite grain boundaries. After warm deformation, specimens were annealed for 2 h at the respective deformation temperature to simulate coiling at elevated temperatures, and then air cooled to room temperature.

To obtain the final ferrite/martensite dual-phase microstructure, all specimens were subjected to intercritical annealing in the ferrite/austenite two-phase region followed by quenching in order to transform all austenite into martensite. This treatment was carried out in a salt bath furnace. The temperature was controlled electronically and held constant at 730 °C. The reheating time was 2 min, as was predetermined using a thermocouple embedded in a test specimen. Samples were annealed for 3 min (including reheating time) in the salt bath, before being quenched in water. The intercritical annealing parameters were established by performing dilatometer tests [29].

Three of the UFG samples were additionally aged at 170 °C for 20 min in a vacuum furnace to simulate the BH process, which is active during paint baking in automotive manufacturing. Generally, the increase in yield strength after prestraining between 2% and 12% plus aging at ∼170 °C for 20–30 min is determined to assess the bake-hardenability of a steel grade. Here, only the BH_0 (no prestrain) value for the UFG-DP steel is reported.

2.2. Microstructure characterization

Samples for SEM and EBSD were prepared by standard mechanical grinding and polishing procedures, finishing with 3 min colloidal silica polishing. To reveal the microstructure for SEM observations, the samples were additionally etched in 1% Nital for 3 s. For high-resolution EBSD measurements, the sample surface has to be extremely clean and free of roughness and deformation in order to obtain high-quality Kikuchi patterns. Therefore, they were electropolished using Struers electrolyte A2 at room temperature (voltage: 30 V; flow rate: 12 s^{-1}; polishing time: 10 s).

The martensite volume fraction and the ferrite grain size were determined on the basis of three SEM micrographs taken at a magnification of ×3000 for the UFG and FG steel and of ×500 for the CG steel. A point-counting method was used to determine the second phase fraction. As it is not possible to differentiate between martensite and austenite on etched specimens in the scanning electron microscope, the second phase fraction was determined as the fraction of martensite plus retained austenite. The retained austenite volume fraction was determined to range between 1 and 3 vol.% based on EBSD measurements. The ferrite mean linear intercept length was determined both in the compression direction and in the rolling direction. The average value determines the ferrite grain size.

EBSD maps were taken on a JEOL JSM 6500F high-resolution, high-intensity scanning electron microscope equipped with a field emission gun (FEG SEM) and for energy-dispersive X-ray analysis. The small beam diameter and its high brightness yield high-contrast Kikuchi patterns with a large signal to noise ratio. In this way, information about small orientation deviations can be obtained, even in deformed areas with high dislocation densities like phase or grain boundaries [35,36]. A high-speed DigiView CCD camera was used for pattern acquisition. Data was recorded and analyzed using the EDAX/TSL OIM software package [37]. The lateral resolution of orientation microscopy using the FEG SEM was shown to be of the order of a few tens of nanometers, depending on the material investigated and the microscope, camera and software parameters used [37]. By choosing the highest possible image resolution for pattern acquisition and by optimizing the parameters of the Hough transformation, an angular resolution of about 0.3° can be obtained [37,38]. The step size was 50 nm for the UFG and FG steels and 200 nm for the CG steel. An acceleration voltage of 15 kV and an emission current of around 80 μA were used for all scans. Martensite was indexed as body-centered cubic ferrite. Due to its higher dislocation density, it can be easily distinguished from ferrite by its significantly lower image quality (IQ) and confidence index. In the present work, the minimum misorientation angle that defines a grain boundary was set to 2°. Misorientation angles between 2° and 15° are called low-angle grain boundaries (LAGBs). Misorientation angles larger than 15° are designated high-angle grain boundaries.

Slip-band evolution was studied on the basis of interrupted tensile tests using flat specimens ($5 \times 60 \times 3$ mm^3). Sections containing rolling and normal directions were prepared by mechanical grinding and polishing. Two microhardness indents were placed within the center region of the specimen as a reference to measure the plastic strain after each tensile step. Micrographs and EBSD maps were taken within this distance. The scan position was easily recognized after each straining step due to the slight surface contamination.

2.3. Tensile testing

Cylindrical tensile test specimens with a diameter of 4 mm and a gage length of 20 mm were machined according to the German Industry Norm DIN 50125-B. Tensile tests were conducted at room temperature with a constant cross-head speed of 0.5 mm min^{-1} and an initial strain rate of 0.5×10^{-3} s^{-1}. Due to the continuous yielding behavior of the DP steels, the yield strength is given as the 0.2% offset yield strength. In the case of the UFG as-received material, the lower yield strength is reported. The uniform elongation was determined as the strain at which the true strain equals the strain-hardening rate (Considère criterion). The strain-hardening exponent, n, was determined as an approximation to the Hollomon equation ($\sigma_t = k\varepsilon_t^n$, where σ_t is the true stress, ε_t is the true strain and k is an empirical constant) between 2% and uniform elongation for the DP steels and between the onset of continuous yielding and uniform elongation for the UFG as-received material. The reduction in area was determined by measuring the area of the fracture surface related to the initial cross section.

3. Results

3.1. Microstructures

The microstructure obtained after hot deformation and air cooling followed by intercritical annealing (CG route) consists of a ferrite matrix with a grain size of 12.4 μm and 31.3 vol.% martensite (Table 1), the latter occurring partly as isolated islands, partly as aligned bands.

By applying multi-pass warm deformation at 700 °C (FG route) and at 550 °C (UFG route) between hot deformation and intercritical annealing, the ferrite grain size is reduced to 2.4 and 1.2 μm, respectively. The martensite fraction is 30.1 vol.% in the FG steel and 29.8 vol.% in the UFG steel. Exemplary micrographs are shown in Fig. 2. Note that the magnification is the same in all images. Upon BH, the microstructure does not change visibly in the scanning electron microscope, the ferrite grain size being 1.2 μm and the martensite volume fraction 28.2%.

As neither the chemical composition nor the intercritical annealing temperature or holding time was changed, all three steels contain similar martensite fractions with presumably similar martensite carbon contents. Using a mass balance calculation, the martensite carbon content C_m can be estimated from the equation:

$$C_m = \frac{C_c - C_f(1 - f_m)}{f_m} \qquad (1)$$

where C_c is the carbon content of the composite, C_f is the carbon content of ferrite and f_m is the martensite volume fraction. The ferrite carbon content was estimated using thermo-calc [39]. It was assumed that, upon water quenching, the ferrite keeps the carbon content that is present at the temperature at which the austenite fraction is 30 vol.%. Thus, ferrite is supersaturated in carbon, the carbon content being 0.01 wt.%. Inserting this value in Eq. (1) yields a martensite carbon content of 0.54 wt.%, assuming that no cementite is present in the microstructure.

Other authors conducting similar investigations [24,27] found that phase transformation kinetics is enhanced upon grain refinement. Hence, they report a higher martensite volume fraction in their UFG materials after the same intercritical annealing treatment. The reason why the martensite volume fraction is nearly the same for all grain sizes in the present case is probably the different processing route applied. Due to the pronounced recovery during large-strain warm deformation, the stored energy in the initial microstructure might be lower than in the materials processed by ECAP or cold swaging. Hence, the driving force for phase transformation is not profoundly enhanced in the present case. This leads to the advantageous situation that in this study the differences in the mechanical properties can be solely attributed to the different grain size and these effects are not overlaid by differences in martensite volume fraction. However, it will be shown in the

Table 1
Microstructure parameters obtained from SEM micrographs and tensile tests presented as average value of three tensile specimens for each material.

Steel	MVF (%)	d_f (μm)	YS (MPa)	UTS (MPa)	UE (%)	TE (%)	RA (%)	Yield ratio	*n*-value
CG	31.3	12.4	445 ± 17	870 ± 25	7.2 ± 0.7	7.7 ± 1.0	13.0 ± 4.4	0.51 ± 0.01	0.21 ± 0.01
FG	30.1	2.4	483 ± 7	964 ± 4	7.4 ± 0.4	8.9 ± 0.8	18.7 ± 2.6	0.50 ± 0.01	0.18 ± 0.01
UFG	29.8	1.2	525 ± 8	1037 ± 15	7.1 ± 0.5	7.3 ± 0.4	15.3 ± 4.0	0.51 ± 0.01	0.18 ± 0.01
UFG-BH	28.2	1.2	619 ± 6	1005 ± 5	8.6 ± 0.2	11.4 ± 1.5	37.5 ± 0.9	0.62 ± 0.003	0.16 ± 0.004
UFG as-received	–	0.8	578 ± 12	633 ± 6	7.3 ± 0.1	13.3 ± 1.2	61.9 ± 4.6	0.91 ± 0.03	0.06 ± 0.001

Standard deviations are given in brackets. MVF: martensite volume fraction; d_f: ferrite grain size (mean linear intercept length); YS: 0.2% offset yield strength; UTS: ultimate tensile strength; UE: uniform elongation; TE: total elongation; RA: reduction in area.

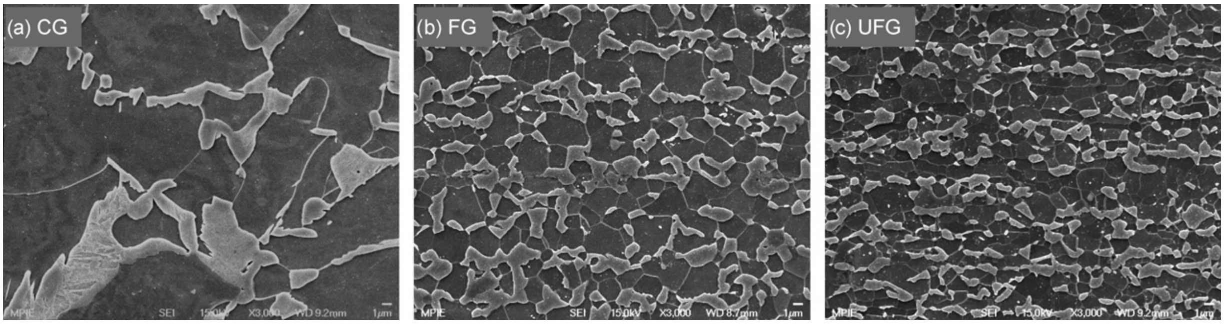

Fig. 2. Microstructures of the (a) CG material (12.4 μm ferrite grain size), (b) FG material (2.4 μm ferrite grain size) and (c) UFG material (1.2 μm ferrite grain size) produced by the processing routes illustrated in Fig. 1 plus intercritical annealing for 3 min at 730 °C in a salt bath, followed by water quenching. As the microstructure does not change visibly upon aging, this microstructure is not shown here.

following that the martensite distribution does have an influence on the mechanical behavior.

3.2. Tensile properties

Fig. 3 shows the engineering stress–strain curves of the CG, FG, UFG and UFG-BH steel. For each material, the result of only one of the three tensile tests is shown, because the variations within each series are rather small (see the standard deviations in Table 1). The CG, FG and UFG steels show the typical characteristics of as-quenched ferrite/martensite dual-phase steels: low elastic limit, absence of a distinct yield point, continuous yielding and high initial strain-hardening rate. With decreasing grain size, the yield strength and the tensile strength are increased remarkably whereas uniform elongation and total elongation are only slightly affected. The BH process affects the mechanical properties in two ways: first, it promotes the reoccurrence of a yield point (though the transition between elastic and plastic deformation is still rather smooth); and second, it enhances the ductility considerably in terms of uniform elongation, total elongation and reduction in area. The tensile strength is slightly reduced due to BH. For comparison, the stress–strain curve of the as-received UFG material is also shown. While the yield strength is slightly higher than in the UFG-DP steel, the strain-hardening rate is much lower, resulting in a relatively low tensile strength. The onset of plastic deformation is characterized by pronounced Lüders straining. The uniform elongation is the same as in the UFG-DP steel, but lower than in the bake-hardened UFG-DP steel. The total elongation is higher than in the other investigated steels; this is ascribed to the large post-uniform plasticity.

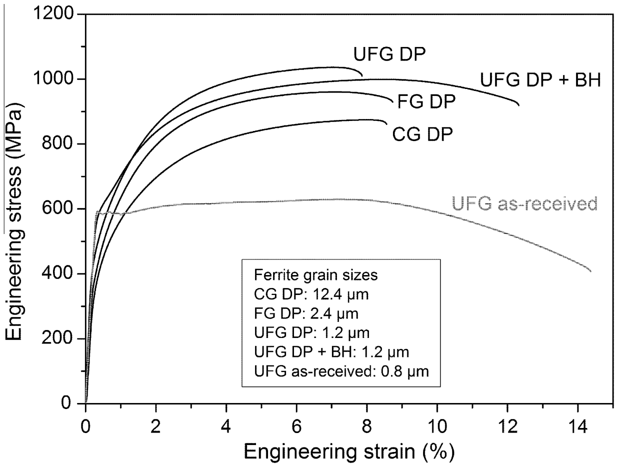

Fig. 3. Exemplary engineering stress–strain curves of the steels with CG, FG and UFG ferrite matrix and of the aged (BH) UFG steel. The UFG ferrite/cementite starting material is also shown. Initial strain rate: 0.5×10^{-3} s^{-1}. DP refers to the term "dual-phase".

Table 1 lists the average values of each steel obtained from three separate tensile tests. The yield strength (0.2% offset yield strength) and tensile strength increase linearly with the inverse square root of the ferrite grain size, i.e. the Hall–Petch relation is obeyed. The grain size dependence (Hall–Petch slope) is 4.0 MPa/$d^{-1/2}$ for the yield strength (with d being the grain diameter in mm), and 8.39 MPa/$d^{-1/2}$ for the tensile strength. As yield and tensile strength are increased by nearly the same factor due to grain refinement, the yield ratio is nearly constant. The bake-hardened UFG steel does not coincide with these trends. The 0.2% offset yield strength is increased by 94 MPa compared to the as-quenched UFG steel and the tensile strength is decreased by 32 MPa, resulting in a change in the yield ratio from 0.51 to 0.62. As the yield point after BH is more pronounced yet still not sharp, it is reasonable to specify the 0.2% offset yield strength rather than the lower yield strength.

The effect of grain refinement on ductility is more complex than its effect on strength. The uniform elongation (Table 1) is nearly constant around 7% for the CG, FG and UFG steels. Bake-hardening increases uniform elongation to around 8.6%. Regarding only the as-quenched materials, both total elongation and reduction in area are highest in the FG steel. The UFG steel has a lower total elongation than the CG steel but a higher reduction in area. However, the differences are rather small. The BH treatment improves the total elongation by 2.5% and – more significantly – the reduction in area by 22.2%.

The analysis of the strain-hardening rate (Fig. 4) reveals that the initial strain-hardening rate is increased by grain refinement but is nearly the same for the FG and UFG steels. At higher strain levels, the two curves converge with the curve of the CG steel, i.e. the effect of grain refinement continuously decreases. The bake-hardened steel starts with lower strain-hardening rates in the range of the CG steel (for $\varepsilon_t > 0.01$). The curve shows a minimum in the initial stage due to the more pronounced yield point. At higher strain levels, it intersects the other curves, achieving a higher uniform strain. The *n*-value, calculated at strain levels between 2% and uniform elongation (Table 1), drops off slightly from 0.21 for the CG steel to 0.18 for the FG and UFG steels and becomes 0.16 for the bake-hardened steel. The *n*-value of all DP steels is considerably larger than in the UFG ferrite/cementite starting material.

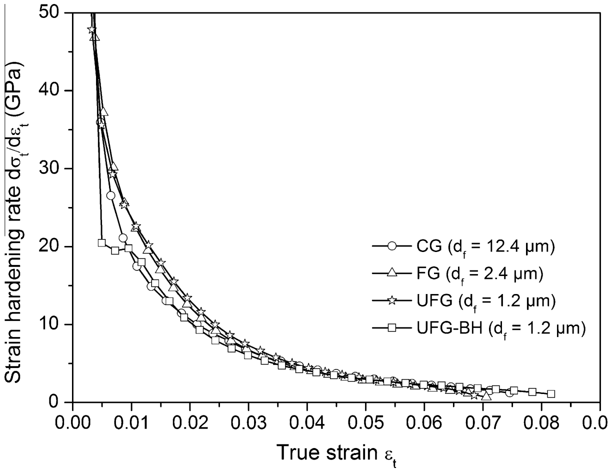

Fig. 4. Strain-hardening rate as a function of true strain. Grain refinement increases the initial strain-hardening rate, whereas BH decreases it. CG, FG, UFG and UFG-BH are as defined in the text.

Fig. 5 shows the tensile specimens after failure. The degree of necking (post-uniform elongation) increases with decreasing grain size and is strongest for the bake-hardened specimens. The micrographs reveal the respective fracture modes of the steels. In the case of the CG steel, it is mainly brittle, which is documented by well-defined facets and cleavage steps on these facets (Fig. 5a). Only some small areas consist of dimples. The latter are located in the martensitic area, whereas the ferrite exhibits cleavage planes, as was observed previously [40,41]. The dominant fracture mode of the FG steel is ductile, although smaller parts of the specimen have undergone brittle fracture (Fig. 5b). The UFG steel shows dimples throughout the specimens, in both the as-quenched (Fig. 5c) and bake-hardened conditions (Fig. 5d). This suggests a failure process of void nucleation and growth, and hence entirely ductile fracture. Some dimples are formed around inclusions.

In order to identify, the preferred void nucleation sites, surfaces perpendicular to the fracture surface were also analyzed. In the CG steel, the main fracture mechanism is martensite cracking. The cracks form mostly in the banded areas perpendicular to the applied tensile strain (Fig. 6a). Most of the cracks stop at the ferrite/martensite interface, but some penetrate into a minor fraction of the adjacent ferrite grain. Martensite fracture was observed at strains as low as 3.4% plastic strain (see below). Void nucleation and growth along ferrite/martensite interfaces occur to a lesser extent within the areas of isolated martensite islands. In the FG and UFG steels, the voids form primarily at ferrite/martensite interfaces and are distributed more homogeneously (Fig. 6b). Martensite cracking takes place less frequently in martensite islands that are of larger than average size and occurs only after necking has started.

3.3. Microstructure evolution during tensile straining

The microstructure evolution during deformation is illustrated for the CG, UFG and UFG-BH steels. The FG steel shows an intermediate deformation behavior. Fig. 7 shows EBSD scans taken perpendicular to the fracture surface of the tensile specimen. In the left column, the IQ maps of areas within the uniform elongation (~7%) are illustrated. The center and right columns show the IQ and inverse pole figure (IPF) maps of areas close to the neck. Martensite is easily identified by its lower IQ and its subdivision into blocks or packets. In all images, the tensile direction (=rolling direction) is horizontal and the normal direction is vertical.

Upon straining to uniform elongation (UE), strain localization in ferrite was observed in the CG steel, as indicated by arrows 1 in Fig. 7a. Locally, a dislocation substructure with vague boundaries has developed (arrow 2). Martensite cracking occurred in some areas (arrow 3). In contrast, the UFG steel shows a less pronounced substructure formation in ferrite. Instead, martensite has undergone considerable deformation and is rotated towards the tensile direction together with the ferrite (arrows in Fig. 7d). The

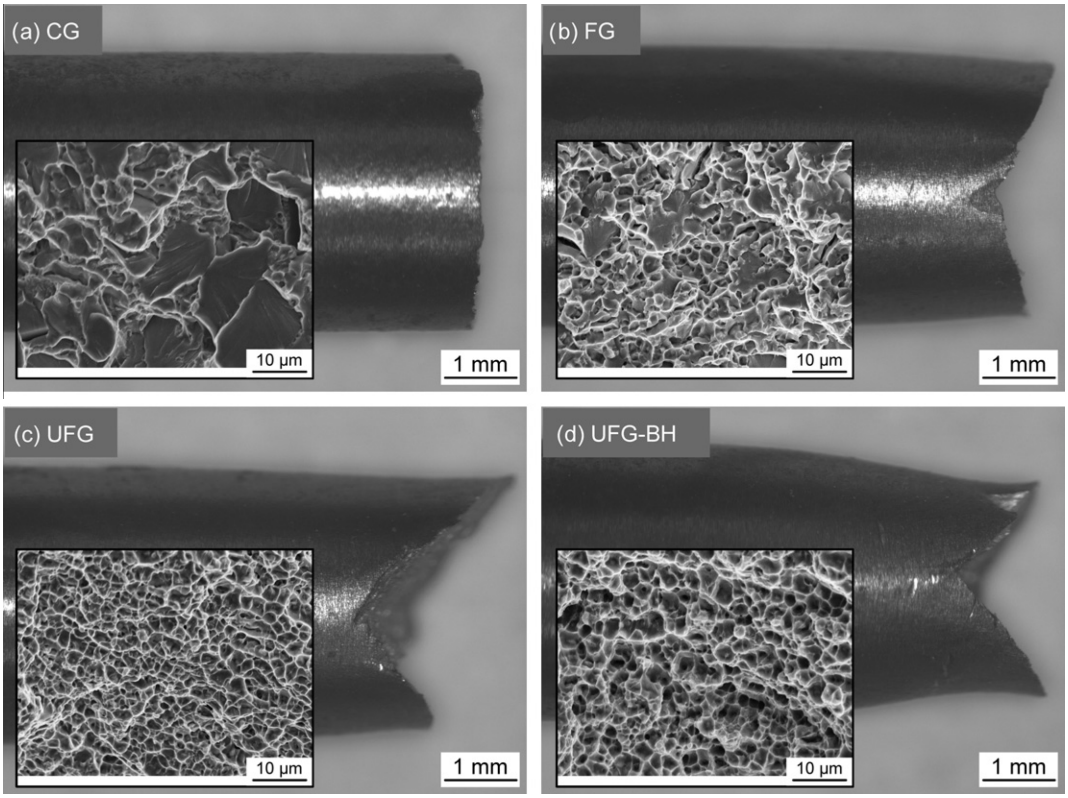

Fig. 5. Tensile specimen after failure showing the increase in post-uniform elongation with decreasing grain size and the promotion of ductile fracture mechanism (a–c). The aging treatment (BH, BH) enhances this trend (d). CG, FG, UFG and UFG-BH are defined in the text.

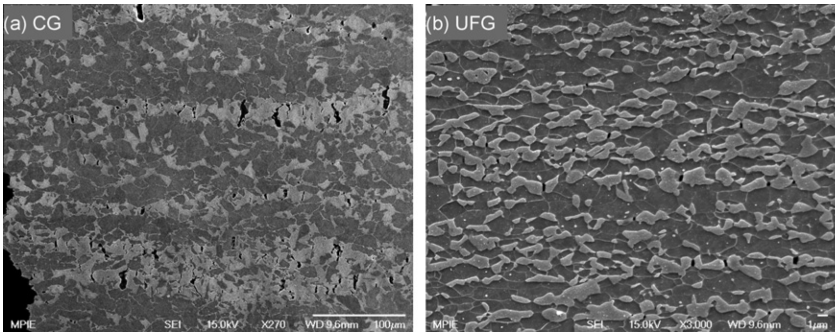

Fig. 6. Observation of the planes perpendicular to the fractured tensile specimen surfaces reveals (a) martensite cracking as the main fracture mechanism in the CG specimen and (b) void nucleation and growth in the UFG specimen. Note the different magnification of the images. The tensile direction is horizontal; the normal direction is vertical.

same is true for the UFG-BH steel. Nevertheless, the martensite is even more deformed compared to the non-bake-hardened state, as is revealed by the more elongated shape of the martensite islands (Fig. 7g).

After failure, strain localization and substructure formation of the CG ferrite is intense, particularly close to ferrite/martensite interfaces. Martensite cracking and interface decohesion are commonplace in this state (arrows in Fig. 7b), while plastic deformation of martensite is not obvious. In the UFG steel (Fig. 7e), it can be easily seen that the martensite is extensively deformed and elongated in the tensile direction. Compared to the CG steel, the deformation substructure in the ferrite is less well developed. Moreover, the distribution of the deformation substructure within the ferrite grains is more homogeneous than in the CG structure. Thus, it seems that strain localization and dynamic recovery are less active in the UFG steel than in the CG steel. On the other hand, the plastic deformation of martensite is more intense. Voids form mainly along the ferrite/martensite interface (arrows in Fig. 7e) and are also elongated in the tensile direction. In the bake-hardened condition, martensite plasticity is

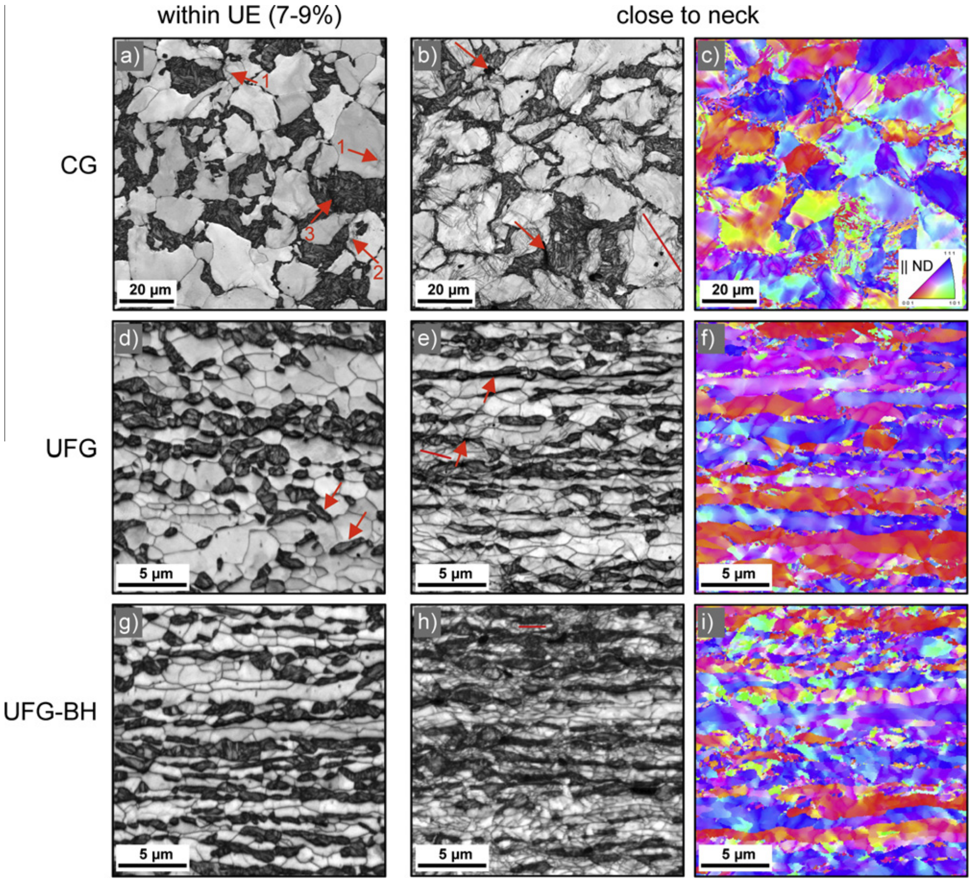

Fig. 7. EBSD maps taken perpendicular to the fracture surface of the CG specimen (a–c), the UFG specimen (d–f) and the UFG-BH specimen (g–i). (a, d, g) IQ maps of areas within the area of UE. IQ maps taken close to the neck (b, e, h) and the respective IPF maps (c, f, i) show the microstructure evolution during straining. The tensile direction is horizontal and equals the rolling direction; the normal direction is vertical.

further enhanced. As indicated by the much higher reduction in area compared to the CG and UFG steels, a subgrain structure is widely developed in the UFG-BH steel.

The IPF maps reflect the different types of strain accommodation in ferrite. The substructure formation in the CG steel results in pronounced orientation gradients which are randomly distributed within the ferrite grains (Fig. 7c), whereas the deformation of the UFG steel results in more planar arrays of crystal orientations in an angle around 40° to the tensile direction (Fig. 7f). The IPF map of the UFG-BH looks similar, yet the subgrain formation is reflected by a finer subdivision of the ferrite grains.

In Fig. 8, typical misorientation profiles of the different ferrite substructures after failure are presented. Their positions are indicated on the respective IQ maps (red[1] lines in Fig. 7b, e and h). From these profiles, it is evident that the UFG-BH sample is the only one which exhibits full development of subgrains that are separated by LAGBs. This is revealed by the stepwise increase in the misorientation angle. The presence of fully developed subgrains indicates that dynamic recovery was active in the necked area of the bake-hardened sample. In the other two specimens, plastic deformation leads to pronounced orientation gradients and to a less extent to well-defined subgrains. This

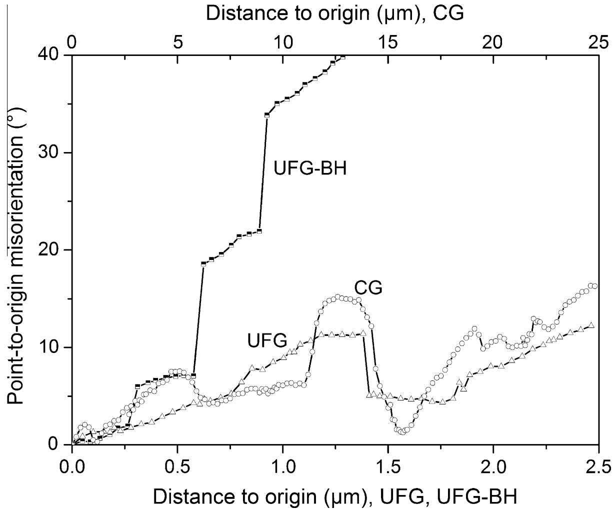

Fig. 8. Point-to-origin misorientation profiles for the UFG and the UFG-BH samples (lower x-axis) compared to CG sample (upper x-axis), taken from EBSD maps close to the neck. Subgrain formation is completed only in the UFG-BH sample.

---

[1] For interpretation of color in Fig. 7, the reader is referred to the web version of this article.

gives rise to more gradually increasing misorientation profiles. Note the different scaling for the CG sample, which indicates a larger size of the subgrains to be formed. The subgrain size of the UFG-BH steel is around 0.3 μm.

The microstructure evolution during deformation was studied in more detail by interrupted tensile tests. The UFG-BH was excluded from this part of the investigation because the tempered state of the microstructure obviously alters the deformation mechanisms and therefore it is not comparable to the untempered state. Although the EBSD scans revealed important information about the deformation substructure, single slip bands cannot be distinguished. Therefore, the evolution of slip bands was studied on polished samples subjected to different strain levels. The CG ferrite exhibits wavy and strongly intersecting slip bands without preferred orientation after 3.4% plastic strain (Fig. 9a). In contrast, the UFG ferrite basically shows two sets of nearly planar slip bands which are oriented around 40° to the tensile direction, as was observed in the IPF maps (Fig. 9b). This suggests that less pronounced orientation gradients are developed in the UFG steel at this strain than in the CG steel, as was observed in the IPF maps in Fig. 7. This assumption was further tested by analyzing the evolution of local misorientations at small strains. For this purpose, the kernel average misorientation (KAM) was used which can be directly retrieved from the EBSD data.

The KAM is defined as the average misorientation angle between an EBSD measurement point and all its neighbors at a certain distance. Given that the KAM angle is strongly dependent on the distance selected, the nearest neighbor used for the calculation was determined based on the following considerations: the distance has to be sufficiently small to ensure that detailed information about local misorientation changes is not ignored and that influences stemming from neighboring grains are not taken into account. At the same time, the distance must allow for averaging out scatter due to the spatial resolution limits of EBSD and for performing the calculations with misorientations above the angular EBSD resolution limit [44]. Hence, for both samples, the CG and the UFG material, neighboring points located at a distance of 200 nm spacing were selected. Misorientation angles above 5° were excluded from the calculation. This angle is large enough to still

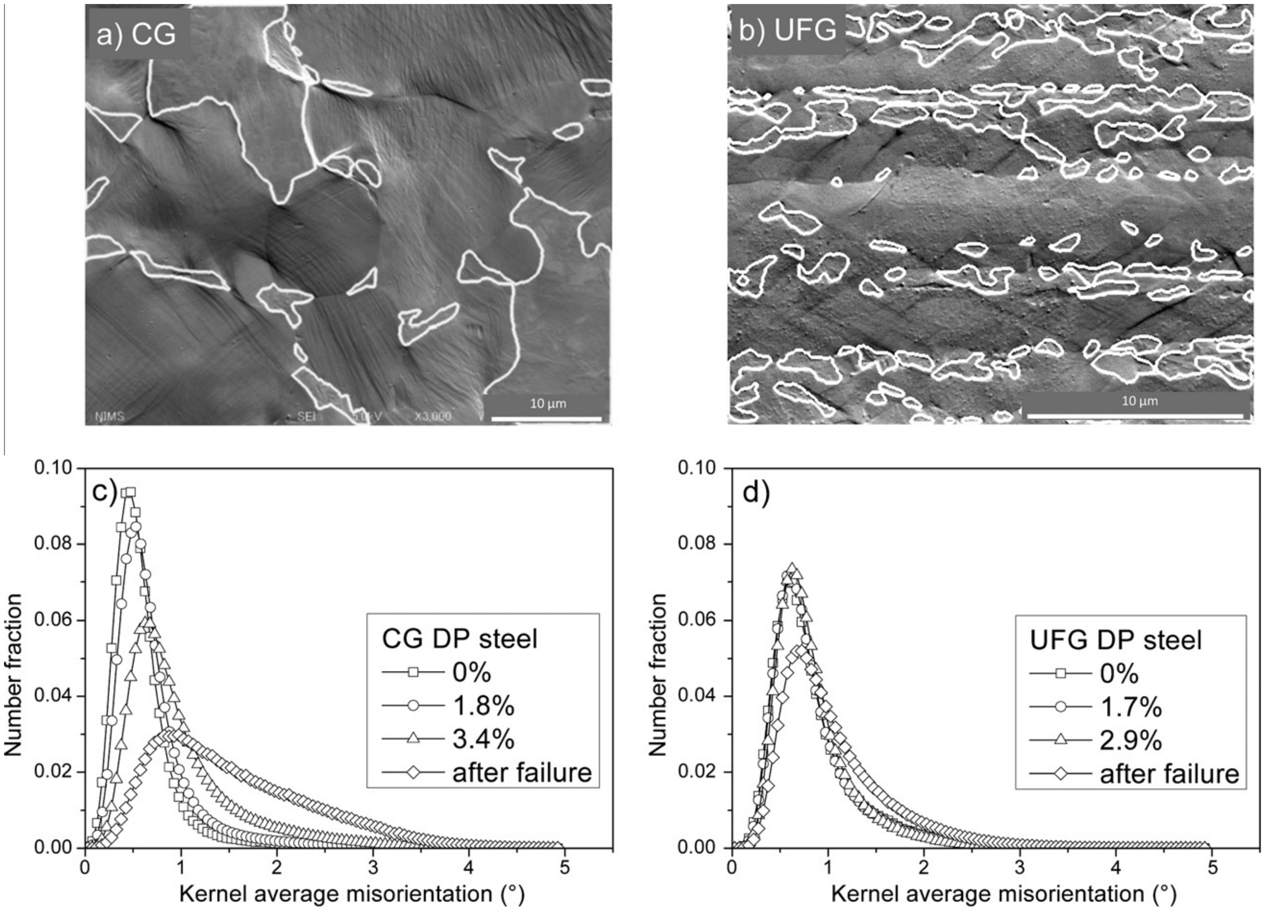

Fig. 9. The CG steel exhibits wavy slip bands (a), whereas slip-band formation in the UFG sample follows a more planar mode (b). The tensile direction is horizontal. The distribution of the KAM values (calculated using neighboring EBSD points at a distance of 200 nm and up to a maximum deviation angle of 5°) at different strain levels in the same sample area shows that lattice rotations take place early during tensile straining in the CG steel (c), whereas they appear delayed in the UFG specimen (d) due to the more constrained plastic deformation in ferrite. The rolling direction is horizontal; the normal direction is vertical.

include in the analysis the subgrains that evolve during plastic deformation, yet is small enough to exclude neighboring grains from the calculation.

The calculation was done at different strain levels on the same sample area. Only the ferrite fraction was taken into account. The results are shown in Fig. 9c and d. In the CG steel, a uniform shift of the peak KAM value to higher misorientation angles and a gradual increase in the fraction of higher misorientation angles are observed. The flattening of the curve indicates that strain is distributed inhomogeneously throughout the ferrite grains. A larger fraction of high misorientation points to the increasing number of dislocation walls or subgrains. The peak value of the KAM at 0% strain is lower in the UFG steel than in the CG steel due to the larger fraction of dislocations at grain boundaries. Up to 3% plastic strain, the KAM distribution remains unchanged. Only after failure was a considerable decrease in the peak value found, accompanied by an increased fraction of high misorientation angles. Hence, the planar slip mode in the UFG steel correlates with restricted lattice rotations and thus delayed subgrain formation. In contrast, non-planar glide, including the intense lattice rotations and earlier formation of a substructure, prevail in the CG steel.

4. Discussion

For the sake of clarity, the discussion of the deformation and fracture mechanisms will focus on the as-quenched specimens only. The effect of BH on deformation and fracture behavior will be addressed in a separate section.

4.1. Deformation mechanisms

In general, the enhancement of strength due to grain refinement is accompanied by a deterioration of ductility. However, it was shown in previous studies [23–28] that this does not apply to DP steels. Instead, it was found that uniform and total elongation are only slightly affected by decreasing ferrite grain size – as was also observed in the present study. This is partly a consequence of the increase in the initial strain-hardening rate with decreasing grain size [25,27,42,43]. In a recent paper [44], the enhancement of the initial strain-hardening rate was explained in terms of reductions in the martensite island size and ferrite grain size. These effects were suggested to enhance the number of dislocation sources and give rise to rapid dislocation interactions. The higher ferrite/martensite phase boundary fraction results in a larger number of GNDs, which are generated during plastic deformation due to the strain incompatibility of the two phases. Furthermore, the back stresses exerted by (i) martensite islands and (ii) ultrafine ferrite grains below 1 μm^3, which are characterized by a more uniform dislocation distribution than larger grains, contribute to the rapid stress increment. It is assumed that the deformation-induced transformation of small amounts of retained austenite plays a secondary role.

When focusing on low strain levels <2%, it must be stated that the increase in yield strength due to ferrite grain refinement contributes to the high initial strain-hardening rate. Due to the absence of a distinct yield point, it is not possible to clearly distinguish between the effect of grain size on strain-hardening rate and that on yield strength. This becomes clear when looking at the strain-hardening rate of the UFG-BH steel, which is nearly equal to the strain-hardening rate of the CG steel. To establish a consistent comparison of the strain-hardening capacity of UFG ferrite/cementite and UFG ferrite/martensite steels, it is thus necessary to analyze UFG ferrite/martensite steels after strain aging, which exhibit a distinct yield point.

The aspect that shall be treated in more detail in the present study is the plasticity of martensite, which is considerably enhanced due to grain refinement. In general, plastic yielding starts in the soft ferrite, with the hard martensite remaining in the elastic state. During the plastic deformation of the ferrite, stress is transferred to the martensite. Internal stresses at the ferrite/martensite interface are built up due to the plastic strain incompatibility. At this stage, the strain-hardening rate is very high as a consequence of rapid dislocation multiplication and the back stresses resulting from the strain incompatibility. When the transferred stress is large enough to reach the elastic limit of the martensite, it starts to deform plastically. Due to the high initial strain hardening of the martensite, the stress increment in the composite is still very high. Only after the martensite flow curve levels off, its contribution to the strain-hardening rate of the composite declines [45]. From these general considerations, it is clear that martensite plasticity is an important factor controlling the overall deformation behavior of DP steels. Generally, the ability of martensite to deform increases with a decay in hardness, which can be reduced by lowering the carbon content or by applying tempering. In view of a composite, a lower strength difference between martensite and ferrite promotes plastic deformation of martensite [46]. Although some studies have reported that plastic deformation of martensite occurs only after uniform elongation (e.g. [42,47]), considerable martensite deformation at lower strains was shown by in situ SEM studies [48,49] and by analyzing the two-stage deformation behavior derived from the strain-hardening rate [25]. In the present materials, both types of behavior have been observed. The martensite in the CG steel seems to remain in the elastic state even in the necked area of the tensile specimen. On the other hand, the FG and UFG steels clearly show considerable martensite deformation before the onset of necking. According to the model developed by Jiang et al. [25], the increase in the yield strength and the strain-hardening rate of the ferrite matrix due to grain refinement results in rapid stress transfer to martensite. Thus, the yield stress of martensite is reached at lower strains than in coarser-grained microstructures. However, it must be assumed that the yield strength of martensite also increases with grain refinement due to the finer packet size. This, in turn, would delay martensite plastic deformation.

In order to identify the reason for the enhanced martensite plasticity due to grain refinement, one has to consider how stress and strain are partitioned between ferrite and martensite. In this respect, the slip-band evolution reveals important information about plastic strain accommodation. In the CG steel, the slip bands appear wavy (Fig. 9a), whereas in UFG steel a more planar slip-band formation is active (Fig. 9b). Planar and wavy slip modes in DP steels were reported by Tomota [50]. Tomota explains the occurrence of planar slip with the restricted operation of plastic relaxation of strain incompatibility while the wavy slip mode is associated with active plastic relaxation. Plastic relaxation can be realized by (i) additional plastic flow in the softer phase, (ii) onset of plastic flow in the harder phase, (iii) fracture of the harder phase or (iv) decohesion at the interface. In the CG steel, plastic relaxation can take place by strain localization and substructure formation in ferrite and by martensite cracking (Fig. 7a and b). Therefore, slip bands develop in a wavy mode (Fig. 9a). This deformation mechanism is accompanied by intense lattice rotations, which are reflected by the gradual increase in local misorientations (Fig. 9c). The finer the ferrite grain size is, the more difficult the plastic deformation of ferrite becomes due to the restricted formation of dislocation pile-ups. The restricted ferrite plasticity is reflected by the planar slip mode (Fig. 9b) and only a few lattice rotations (Fig. 9d). Due to the nearly spherical shape and the resulting high toughness of the martensite islands, both interface decohesion and cracking are impeded at low strains. At later stages of plastic deformation (more than 3%), plastic relaxation in the UFG steel occurs by the onset of martensite plastic flow and by interface decohesion (Fig. 7e). Hence, the plasticity of martensite is strongly dependent on the plastic constraints in the ferrite. The plastic constraint imposed on UFG ferrite is balanced by the more spherical morphology of UFG martensite compared to the CG martensite, the latter often covering ferrite grain boundaries. At a constant martensite volume fraction, the spherical shape toughens martensite and increases the ductility of the composite. Therefore, the UFG steel shows ductility comparable to that of the CG steel at much higher strength levels due to the advantageous morphology and distribution of martensite and the ability of martensite to deform plastically as a response to the restricted plasticity in ferrite.

It is evident from these observations that stress/strain partitioning, which is essential in this type of composite structure, changes significantly upon grain refinement. In the CG steel, stress/strain partitioning is extensive in the sense that martensite carries the major part of the stress and ferrite carries the major part of the strain. This leads to strain localization in ferrite and to early cracking of martensite. Upon grain refinement, ferrite is strengthened more than martensite, as the yield strength of martensite is mainly a function of its carbon content, which is supposed to be nearly constant in all investigated materials. In particular, ferrite grains below 1 μm^3 will act as a load-carrying phase. Using three-dimensional EBSD measurements, these grains were shown to be often entirely prestrained by the volume expansion accompanying the austenite-to-martensite phase transformation [44]. Thus, the hardness difference between ferrite and martensite is presumably decreased due to grain refinement. In this situation, the hard phase (martensite) is forced to undergo plastic deformation at lower strains [45]. Thus, stress and strain are partitioned more evenly between martensite and ferrite in the UFG material. This leads to less severe strain incompatibility at the ferrite/martensite interface, resulting in better interface cohesion, and therefore to delayed void formation and an improved post-uniform elongation (Fig. 5).

More research is needed to fully understand the deformation mechanisms in this UFG composite structure. In this respect, digital image correlation is a suitable technique to quantify the strains accommodated by ferrite and martensite [48,51], and will be applied in the future. Furthermore, the hardness difference between ferrite and martensite in the different materials shall be quantified using nanoindentation.

4.2. Fracture mechanisms

Grain refinement promotes ductile fracture mechanisms (Fig. 5). In the CG material, brittle fracture behavior is favored due to martensite banding, a large martensite island size and unfavorable distribution along ferrite grain boundaries. Voids and cracks are distributed mainly around martensite bands (Fig. 6), where local stresses concentrate. As stress is transferred to martensite during tensile straining of DP steels, the fracture stress in martensite is reached much earlier than in ferrite. Therefore, fracture of martensite is initiated. Martensite cracking is facilitated by (i) the low toughness of the martensite islands and (ii) the presence of former austenite–austenite grain boundaries, which are known to be brittle due to their high susceptibility to segregations [52]. The initiated microcracks impose a high shear stress on the neighboring ferrite, which increases with the martensite effective grain size. Hence, failure of coarse martensite islands leads to cleavage fracture of ferrite [53]. As a consequence, premature martensite cracking controls both tensile strength and uniform elongation in the CG steel.

In the FG and UFG steels, martensite cracking is less frequent as a result of the enhanced martensite plasticity and the better interface cohesion as described above. By deforming, martensite releases part of the local stress concentrations and retards void formation, which results in higher fracture strains. Moreover, it is known that the plastic strain needed for the failure of a particle (or grain) increases with decreasing particle size. This is explained by the smaller number of dislocations piling-up at grain and phase boundaries, which result in lower shear stresses [41]. If martensite failure occurs, the produced cracks are not large enough to initiate cleave fracture of the adjacent ferrite. This is because the length of the crack, which determines the peak stress at the crack tip, is restricted by the grain size. Thus, grain refinement increases the cleavage fracture stress and promotes ductile fracture mechanisms at room temperature.

These findings are similar to the results of Kim and Thomas [54], who found that coarse DP structures fracture predominantly by cleavage, while both fine fibrous and fine globular structures fracture in a ductile manner. They attribute this behavior to the constrained possibility of deformation localization in the fine structures, which reduces the probability of cleavage crack nucleation in ferrite. Indeed, the observed strain localization in the CG material is likely to induce cleavage fracture in ferrite. As less excess strain is generated in UFG ferrite, less excess stress is exerted on the martensite phase. Thus, the more even stress and strain partitioning promotes the void nucleation and growth process that is characteristic of ductile fracture behavior. In the CG steel, more stress is transferred to martensite, leading to premature local fracture of martensite and mainly brittle fracture behavior with nearly absent post-uniform elongation.

4.3. Aging response of the UFG material

The BH (aging) process induces static strain aging phenomena in the ferrite and tempering phenomena in the martensite [55]. Carbon atoms in solid solution form Cottrell atmospheres around dislocations and grain boundaries or precipitate as transition carbides in ferrite and/or martensite [56]. The diffusion of carbon includes a volume decrease in martensite, which reduces the internal stresses in ferrite. The formation of Cottrell atmospheres around dislocations causes (partial) pinning of these dislocations. In addition to the reduction in internal stresses, this leads to the reoccurrence of a more distinct yield point and to an increase in the yield strength. In the present case, no sharp yield point was regenerated after BH, but the 0.2% offset yield strength increases by nearly 100 MPa. The dislocation pinning and release of internal stresses successfully suppressed the early onset of plastic deformation of ferrite. The strengthening effect of carbon precipitation is accompanied by a loss in hardness due to the removal of supersaturated carbon in solid solution. This effect might be the reason for the reduction in tensile strength by 32 MPa after BH. Similar findings were proposed by Tanaka et al. [57], who attribute the decrease in tensile strength to the reduction in the amount of excessively dissolved carbon in ferrite. This was experimentally confirmed by Nakaoka et al. [58]. The combined effects of the increase in yield strength and decrease in tensile strength are assumed to be the reason for the lower strain-hardening rate compared to the non-bake-hardened steel (Fig. 4).

The effect of BH on yield strength is more pronounced than on tensile strength, which is consistent with the findings on CG DP steels [59]. The common explanation is that aging phenomena, including the formation of Cottrell atmospheres around dislocations, mainly affect the onset of yielding by restricting the dislocation motion, thereby increasing the yield strength. As soon as the dislocations tear off the Cottrell atmospheres, yielding and strain hardening are controlled by dislocation motion and multiplication, as well as by the hardness difference between the phases. Hence, aging phenomena play a minor role in the strain range of the tensile strength.

The most remarkable effect of BH is the increase in total elongation and reduction in area. One reason for the increased ductility might be the above-mentioned decrease in ferrite hardness due to a loss of dissolved carbon, as was suggested by Koo and Thomas [60]. The other reason is the decrease in martensite hardness due to tempering effects. Decreasing the hardness of martensite increases the critical strain required for interface decohesion or martensite cracking. As a consequence, extensive deformation of martensite was found in the necked area of the tensile specimen (Fig. 7h). As the martensite plasticity retards the formation of voids, plastic deformation of ferrite can continue. Therefore, a rather homogeneous subgrain structure in the ferrite is formed close to the necking zone of the UFG-BH sample (Figs. 7h and 8). The beneficial effect of tempering on decreasing the strength of martensite and, therefore, promoting its plastic deformation was documented for coarser-grained microstructures by Kang et al. [48] and Mazinani and Poole [61].

5. Conclusions

Three low-carbon dual-phase steels with nearly constant martensite fraction around 30 vol.% martensite and different ferrite grain sizes (1.2, 2.4 and 12.4 μm) were produced by applying hot deformation and large-strain warm deformation at different deformation temperatures, followed by intercritical annealing. Their deformation and fracture mechanisms were studied based on tensile test data and microstructure observations. The BH response was investigated for the UFG steel. The main conclusions are:

- Grain refinement leads to an increase in both yield strength and tensile strength following a linear relationship of the Hall–Petch type. Uniform elongation and total elongation are hardly affected. The initial strain-hardening rate and the reduction in area increase as the grain size decreases.
- The increase in the initial strain-hardening rate due to grain refinement is attributed to early dislocation interactions, the high number of dislocation sources and the back stresses exerted by (i) martensite islands and (ii) very small ferrite grains below 1 μm^3.
- Aging at 170 °C (bake-hardening) of the UFG steel leads to a strong increase in yield strength and a small decrease in tensile strength. Ductility is enhanced in terms of uniform and total elongation. Reduction in area is improved by 22% (from 15.3% to 37.5%). These effects are attributed to dislocation locking, relaxation of

internal stresses, reduction in supersaturated interstitial carbon content in ferrite and tempering effects in martensite.

- Grain refinement leads to plastic constraints in the ferrite matrix, which is reflected by homogeneous planar slip-band arrays. Strain localization in CG ferrite is accomplished by wavy slip bands. The wavy slip mode leads to pronounced lattice rotations and early formation of a substructure in CG ferrite, whereas the planar slip mode provokes less lattice rotations. The plastic constraints in FG and UFG ferrite force martensite to deform plastically earlier during tensile straining, whereas strain localization and subgrain formation are impeded.
- The increase in strength at improved ductility due to grain refinement is attributed to the combined effect of strengthened ferrite and enhanced toughness of martensite. This leads to less severe stress/strain partitioning and better interface cohesion.
- Grain refinement promotes ductile fracture mechanisms. Besides the beneficial effects of less excess strain in ferrite and less excess stress in martensite, the formation of martensite cracks and cleavage fracture in ferrite is suppressed in the FG and UFG steels due to the small size, the more homogeneous distribution and the more spherical shape of martensite islands.

References

[1] Howe AA, et al. ECSC contract 7210.PR/167. Luxembourg: EC; 2000.
[2] Song R, Ponge D, Raabe D, Speer JG, Matlock DK. Mater Sci Eng A 2006;441:1.
[3] Hodgson PD, Hickson MR, Gibbs RK. Mater Sci Forum 1998;284–302:63.
[4] Song R, Ponge D, Raabe D, Kaspar R. Acta Mater 2005;53:845.
[5] Yada H, Matsumura Y, Nakajima K. US patent 4466,842. Tokyo, Japan: Nippon Steel Corporation; 1984.
[6] Ohmori A, Torizuka S, Nagai K. ISIJ Int 2004;44:1063.
[7] Ueji R, Tsuji N, Minamino Y, Koizumi Y. Acta Mater 2002;50:4177.
[8] Valiev RZ, Langdon TG. Prog Mater Sci 2006;51:881.
[9] Saito Y, Utsunomiya H, Tsuji N, Sakai T. Acta Mater 1999;47:579.
[10] Ivanisenko Y, Lojkowski W, Valiev RZ, Fecht HJ. Acta Mater 2003;51:5555.
[11] Park KT, Shin DH. Metall Mater Trans A 2002;33:705.
[12] Hanamura T, Yin F, Nagai K. ISIJ Int 2004;44:610.
[13] Song R, Ponge D, Raabe D. Acta Mater 2005;53:4881.
[14] Azizi-Alizamini H, Militzer M, Poole WJ. Scr Mater 2007;57:1065.
[15] Zhang ZL, Liu YN, Zhu JW, Guang YU. Mater Sci Forum 2007;551–552:199.
[16] Shin DH, Park K-T. Mat Sci Eng A 2005;410–411:299.
[17] Hayami S, Furukawa T. In: Korchynsky M, editor. Microalloying 75 proceedings of an international symposium on high-strength, low-alloy steels. New York: Union Carbide Corporation; 1977. p. 311.
[18] Speich GR, Miller RL. In: Kot RA, Morris JW, editors. Structure and properties of dual-phase steels. New York: The Metallurgical Society of AIME; 1979. p. 145.
[19] Moyer JM, Ansell GS. Metall Trans A 1975;6:1785.
[20] Bourell DL, Rizk A. Acta Metall 1983;31:609.
[21] Davies RG. Metall Trans A 1978;9:41.
[22] Rigsbee JM, Vander Arend PJ. In: Davenport AD, editor. Formable HSLA and dual-phase steels. New York: The Metallurgical Society of AIME; 1979. p. 58.
[23] Chang PH, Preban AG. Acta Metall 1985;33:897.
[24] Delincé M, Brechet Y, Embury JD, Geers MGD, Jacques PJ, Pardoen T. Acta Mater 2007;55:2337.
[25] Jiang ZH, Guan ZZ, Lian JS. Mater Sci Eng A 1995;190:55.
[26] Mukherjee K, Hazra SS, Militzer M. Metall Mater Trans A 2009;40A:2145.
[27] Son YI, Lee YK, Park KT, Lee CS, Shin DH. Acta Mater 2005;53:3125.
[28] Tsipouridis P, Werner E, Krempaszky C, Tragl E. Steel Res Int 2006;77:654.
[29] Calcagnotto M, Ponge D, Raabe D. ISIJ Int 2008;48:1096.
[30] Mukherjee K, Hazra S, Petkov P, Militzer M. Mater Manuf Process 2007;22:511.
[31] Song R. Microstructure and mechanical properties of UFG C–Mn steels. Aachen: Shaker Verlag; 2005.
[32] Song R, Ponge D, Raabe D. ISIJ Int 2005;45:1721.
[33] Kaspar R, Pawelski O. Materialprüfung 1989;31:14.
[34] Pawelski O, Kaspar R. Materialprüfung 1988;30:357.
[35] Humphreys FJ. J Mater Sci 2001;36:3833.
[36] Schwartz AJ, Kumar M, Adams BL, Field DP. Electron backscatter diffraction in materials science. New York: Springer; 2009.
[37] Dingley D. J Microsc-Oxford 2004;213:214.
[38] Bate PS, Knutsen RD, Brough I, Humphreys FJ. J Microsc-Oxford 2005;220:36.
[39] Jansson B, Schalin M, Selleby M, Sundman B. In: Bale CW, Irons GA, editors. Computer software in chemical and extractive metallurgy. Quebec: The Metallurgical Society of CIM; 1993. p. 57.
[40] Cai XL, Feng J, Owen WS. Metall Trans A 1985;16:1405.
[41] He XJ, Terao N, Berghezan A. Met Sci 1984;18:367.
[42] Balliger NK, Gladman T. Met Sci 1981;15:95.
[43] Calcagnotto M, Ponge D, Raabe D. Mater Sci Eng A 2010;527:7832–40. doi:10.1016/j.msea.2010.08.062.
[44] Calcagnotto M, Ponge D, Demir E, Raabe D. Mater Sci Eng A 2010;527:2738.
[45] Fischmeister H, Karlsson B. Z Metallkd 1977;68:311.
[46] Lian J, Jiang Z, Liu J. Mater Sci Eng A 1991;147:55.
[47] Marder AR. Metall Trans A 1982;13:85.
[48] Kang JD, Ososkov Y, Embury JD, Wilkinson DS. Scr Mater 2007;56:999.
[49] Su YL, Gurland J. Mater Sci Eng 1987;95:151.
[50] Tomota Y. Mater Sci Technol 1987;3:415.
[51] Ghadbeigi H, Pinna C, Celotto S, Yates JR. Mater Sci Eng A 2010;527:5026.
[52] Becker J, Hornbogen E, Stratmann P. Z Metallkd 1980;71:27.
[53] Uggowitzer P, Stüwe HP. Mater Sci Eng 1982;55:181.
[54] Kim NJ, Thomas G. Metall Trans A 1981;12:483.
[55] Waterschoot T, Verbeken K, De Cooman BC. ISIJ Int 2006;46:138.
[56] Speich GR, Miller AB. In: Kot RA, Bramfitt BL, editors. Fundamentals of dual-phase steels. New York: The Metallurgical Society of AIME; 1981. p. 279.
[57] Tanaka T, Nishida M, Hashiguchi K, Kato T. In: Kot RA, Morris JW, editors. Structure and properties of dual-phase steels. New York: The Metallurgical Society of AIME; 1979. p. 221.
[58] Nakaoka K, Hosoya Y, Ohmura M, Nishimoto A. In: Kot RA, Morris JW, editors. Structure and properties of dual-phase steels. New York: The Metallurgical Society of AIME; 1979. p. 330.
[59] Davies RG. Metall Trans A 1979;10:1549.
[60] Koo JY, Thomas G. In: Davenport AD, editor. Formable HSLA and dual-phase steels. New York: The Metallurgical Society of AIME; 1979. p. 40.
[61] Mazinani M, Poole WJ. Metall Mater Trans A 2007;38A:328.